ACS NANO
Cite This: ACS Nano 2019, 13, 9936–9943
www.acsnano.org

ARTICLE

Switching the Spin on a Ni Trimer within a Metal–Organic Motif by Controlling the On-Top Bromine Atom

Lei Xie,[†,¶] Haiping Lin,[‡,¶] Chi Zhang,[†] Jingcheng Li,[§] Nestor Merino-Díez,[§,⊥] Niklas Friedrich,[§] Xavier Bouju,[∥] Youyong Li,[‡] Jose Ignacio Pascual,[*,§,#] and Wei Xu[*,†]

[†]Interdisciplinary Materials Research Center, College of Materials Science and Engineering, Tongji University, Shanghai 201804, People's Republic of China

[‡]Institute of Functional Nano & Soft Materials (FUNSOM), Jiangsu Key Laboratory for Carbon-Based Functional Materials & Devices, Joint International Research Laboratory of Carbon-Based Functional Materials and Devices, Soochow University, 199 Ren'ai Road, Suzhou 215123, Jiangsu, People's Republic of China

[§]CIC nanoGUNE, 20018 San Sebastián-Donostia, Spain

[⊥]Donostia International Physics Center (DIPC), 20018 San Sebastián-Donostia, Spain

[∥]CEMES-CNRS, Université de Toulouse, 31000 Toulouse, France

[#]Ikerbasque, Basque Foundation for Science, 48013 Bilbao, Spain

Supporting Information

ABSTRACT: **Controlling the spin of metal atoms embedded in molecular systems is a key step toward the realization of molecular electronics and spintronics. Many efforts have been devoted to explore the influencing factors dictating the survival or quenching of a magnetic moment in a metal–organic molecule, and among others, the spin control by axial ligand attachments is the most promising. Herein, from the interplay of high-resolution scanning tunneling microscopy imaging/manipulation and scanning tunneling spectroscopy measurements together with density functional theory calculations, we successfully demonstrate that a Ni trimer within a metal–organic motif acquires a net spin promoted by the adsorption of an on-top Br atom. The spin localization in the trimetal centers bonded to Br was monitored *via* the Kondo effect. The removal of the Br ligand resulted in the switch from a Kondo ON to a Kondo OFF state. The magnetic state induced by the Br ligand is theoretically attributed to the enhanced Br $4p_z$ and Ni $3d_{z^2}$ states due to the charge redistribution. The manipulation strategy reported here provides the possibility to explore potential applications of spin-tunable structures in spintronic devices.**

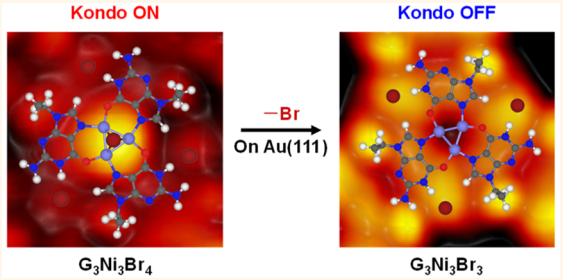

KEYWORDS: *scanning tunneling microscopy, scanning tunneling spectroscopy, Kondo effect, spin switching, ligand attachment, density functional theory*

Controlling the charge and spin at a single molecular scale is a key step toward the realization of molecular electronics and spintronics.[1−5] When a molecular spin lies in the proximity of a metal substrate, it may exhibit the Kondo effect,[6,7] originating from the screening of the localized spin by conducting electrons. This fundamental effect provides an ideal workbench for identifying magnetic atomic and molecular species on surfaces,[8,9] in break junctions,[10,11] as well as in single-electron transistors.[12−17] Its detection has been used as a fingerprint of paramagnetism in systems such as in C_{60},[17] carbon nanotubes,[18] graphene,[19] and different edge states of graphene nanoribbons obtained by on-surface synthesis.[20] Scanning tunneling microscopy (STM) has been proven to be a powerful tool in the characterization of the spin state in magnetic systems.[21−27] Many efforts have been devoted to understanding the influencing factors behind the survival of a molecular spin in contact with a metal surface[28] and determining basic rules for their manipulation. For example, numerous studies of organometallic species with a single metal center, such as metalloporphyrin and -phthalocyanine molecules, reported that the molecular spin can be manipulated by tuning the periphery chemical environ-

Received: June 16, 2019
Accepted: August 5, 2019
Published: August 5, 2019

DOI: 10.1021/acsnano.9b04715
ACS Nano 2019, 13, 9936–9943

Scheme 1. Schematic Illustration of the On-Top Br Atom Induced Kondo Effect on a Three-Metal Center within a Metal–Organic Structure.[a]

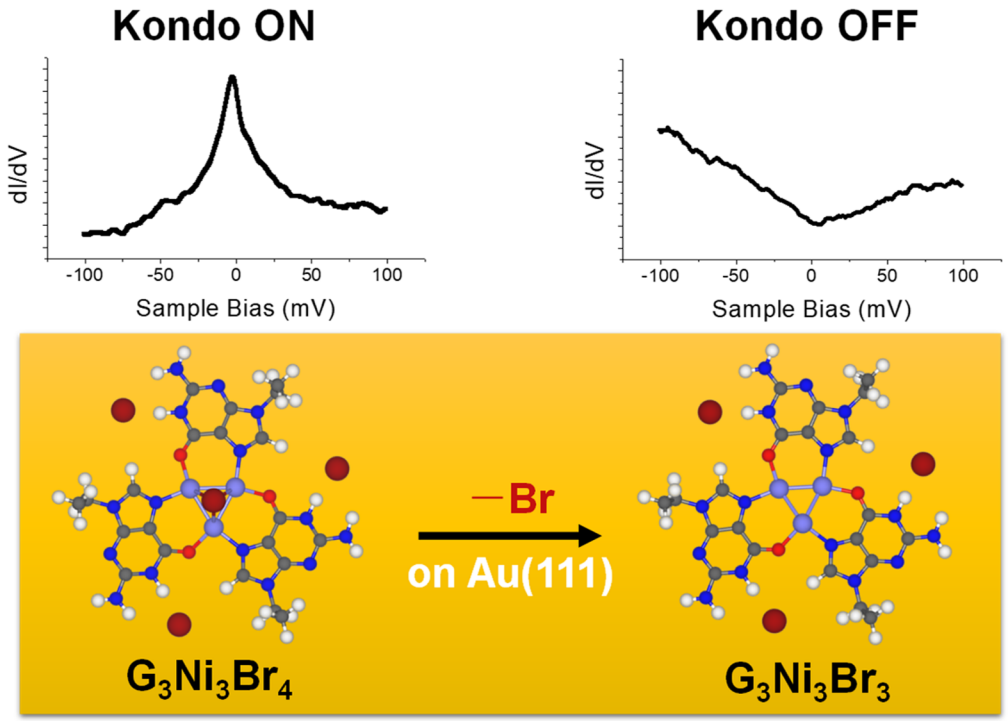

[a]Kondo effect is generated by the attachment of a Br atom above the Ni_3 cluster within the $G_3Ni_3Br_4$ motif on the Au(111) surface. After annealing or STM manipulation, the on-top Br atom is removed and the Kondo effect vanishes in the resulted $G_3Ni_3Br_3$ motif.

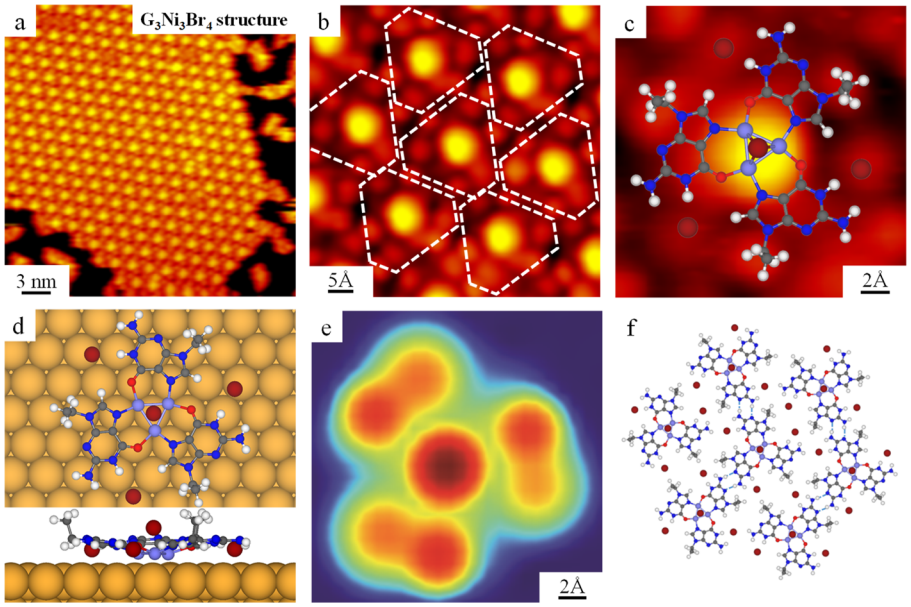

Figure 1. Formation of the $G_3Ni_3Br_4$ network structure after the deposition of G molecules and $NiBr_2$ on Au(111) held at RT. (a) Large-scale STM image showing the close-packed island composed of the $G_3Ni_3Br_4$ structure. (b) Close-up STM image showing the details of the structure in which $G_3Ni_3Br_4$ structures are indicated by white contours. (c) Further zoomed-in STM image of the $G_3Ni_3Br_4$ motif superimposed with the DFT-optimized gas-phase model. (d) Top and side views of the DFT-relaxed model of the $G_3Ni_3Br_4$ motif on Au(111). H, white; C, gray; N, blue; O, red; Ni, light blue; Br, brown; Au, yellow. (e) ESQC calculated STM image of the $G_3Ni_3Br_4$ motif at E_f. (f) DFT-optimized gas-phase model of the $G_3Ni_3Br_4$ network structure. Hydrogen bonds are depicted by blue dashed lines.

ment,[29−33] conformational change,[34−36] the adsorption site on a substrate,[37−39] the structure of the self-assembled domain,[35,40,41] and the axial coordination.[5,42−46] In particular, the possibility of modifying the Kondo state of a magnetic molecule by changing its axial ligand coordination with the attachment of small molecules such as atomic hydrogen,[5] Cl,[42] CO,[43,44] NO,[43] NH_3,[45] and alkali metals[46] has attracted a lot of attention due to the potential applications as gas sensors.

DOI: 10.1021/acsnano.9b04715
ACS Nano 2019, 13, 9936−9943

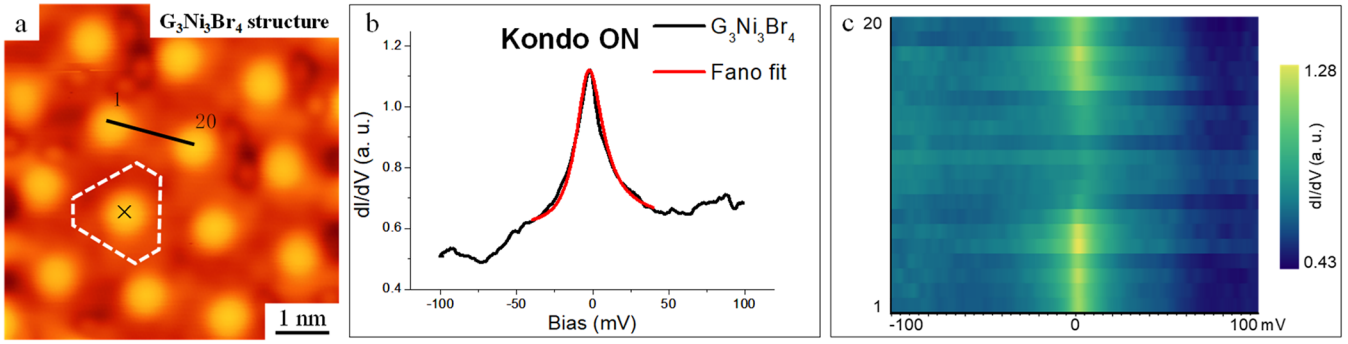

Figure 2. Characterization of the electronic properties of the $G_3Ni_3Br_4$ structure. (a) STM image with a $G_3Ni_3Br_4$ motif highlighted by the white contour. (b) Representative experimental dI/dV point spectrum (the black curve) obtained at the black cross shown in (a), which shows a pronounced peak at the Fermi level representing the signature of Kondo effect (open-feedback parameters: V_t = 1.0 V, I_t = 1 nA, modulation voltage V_{rms} = 0.4 mV, lock-in frequency = 760 Hz); the corresponding Fano fit curve (the red one) (q = 10, Γ = 10.8 mV) shows good agreement. The flat density of states of the STM tip is checked before and after on the bare Au(111) surface, where it only displays the well-known surface state onset (Figure S1). (c) Spectral map of 20 spectra taken along the black line in (a) stacked vertically with colors corresponding to dI/dV intensity.

However, the study of the magnetic ground state of multiple metal centers into complex assemblies is still elusive, as well as the development of possible manipulation routes that could enable/disable their Kondo screening with the substrate. These would prompt the design of devices for electrical sensing of chemical signals.

In this study, we report the manipulation of the magnetic state of a multiple-metal center in a molecular assembly by addition/removal of Br atoms. Based on our previous study,[47] we chose a derivative of the guanine molecule (9-ethylguanine, abbreviated as G) and a $NiBr_2$ salt with the aim of fabricating a three-metal-center (*i.e.*, Ni trimer, shortened as Ni_3) metal–organic system on the Au(111) surface. Through a combination of high-resolution STM, scanning tunneling spectroscopy (STS), density functional theory (DFT) calculations, and STM image simulations, we demonstrate that this system shows an intermediate configuration with a Br atom sitting on top of the hollow site of the central Ni_3 cluster, which modifies the electronic configuration of the three-metal center. When annealed to higher temperatures, the $G_3Ni_3Br_4$ metal–organic network is transformed into $G_3Ni_3Br_3$, where the on-top Br atom vanishes. Moreover, *in situ* removal of the on-top Br atom by STM manipulation is also achieved. Differential conductance (dI/dV) spectra on the $G_3Ni_3Br_4$ structures show a pronounced zero-bias peak at the Fermi level assigned to the signature of a Kondo effect, which is absent on the $G_3Ni_3Br_3$ structures (Scheme 1); thus, removal of on-top Br atoms of the $G_3Ni_3Br_4$ structure through annealing or *in situ* STM manipulation removes the zero-energy Kondo resonance. Such an on-top Br adsorption induced Kondo effect on a Ni_3 cluster within a metal–organic structure is theoretically interpreted by a charge redistribution over d orbitals of Ni, leading to the gain of a net magnetization.

RESULTS AND DISCUSSION

The co-deposition of G molecules and $NiBr_2$ on the Au(111) surface held at room temperature (RT) results in close-packed islands like the one shown in Figure 1a. A close-up STM image allows us to identify the elementary structural motifs, depicted by white contours in Figure 1b. The characteristic motifs (Figure 1c) are composed of a bright dot at the center, assigned to an on-top Br atom and six peripheral protrusions around the triangular base.[42] This assignment is also confirmed by the Br removal experiment discussed below. The structural motif beneath the central Br atom coincides in size and shape with the structure of the basic motif of $G_3Ni_3I_3$ assemblies reported previously.[47] Thus, we tentatively assign the $G_3Ni_3Br_4$ motif (Figure 1c) to a structure formed by a $G_3Ni_3Br_3$ base with an additional Br atom sitting on the hollow site of the central Ni_3 cluster. This structure is successfully reproduced by DFT structural simulations for a $G_3Ni_3Br_4$ cluster on the Au(111) surface, resulting in the optimized structural model superimposed on the STM image in Figure 1c and depicted in Figure 1d. According to this, the motif is composed of three homochiral G molecules coordinated with three Ni atoms located at the hollow sites of the Au(111) surface. Three peripheral Br atoms are uniformly located at the specific hydrogen-rich harbors *via* electrostatic interactions. Importantly, the top Br atom sits on top of the hollow site of the Ni_3 cluster, with an adsorption energy of −1.40 eV. The corresponding elastic scattering quantum chemistry (ESQC) calculated STM image, shown in Figure 1e, reproduces the major details of our STM images with a large central spot corresponding to the Br–Ni_3 motif, which is brighter than both the lateral ethyl groups and the on-surface Br atoms. The $G_3Ni_3Br_4$ motifs are then linked together by hydrogen bonds and van der Waals interactions to form extended metal–organic islands, as shown in Figure 1f.

As we will show next, the axial attachment of a Br atom on top of the Ni_3 cluster has important consequences on their electronic configuration. First, STS measurements uncover a net magnetization of the $G_3Ni_3Br_4$ metal–organic motif. Figure 2b shows a representative dI/dV point spectrum taken on top of the central Br atom (*cf.* the black cross in Figure 2a), which shows a pronounced, narrow peak centered at zero bias. Based on both the bias position and the logarithmic-like shape of the peak, we attribute it to an Abrikosov–Suhl resonance due to the Kondo effect[21] and named as Kondo resonances herein. The coupling between the magnetic center and surrounding free electrons has further been quantified by fitting the Kondo resonance with a Fano function[48,49] (see details in the Supporting Information), obtaining a Kondo temperature of $T_K \sim 124$ K. The extension of the Kondo signal in STM experiments has been related to the spin localization.[50,51] Accordingly, we conducted 20 dI/dV point spectra along a line between two adjacent on-top Br atoms (black line indicated in

DOI: 10.1021/acsnano.9b04715
ACS Nano 2019, 13, 9936–9943

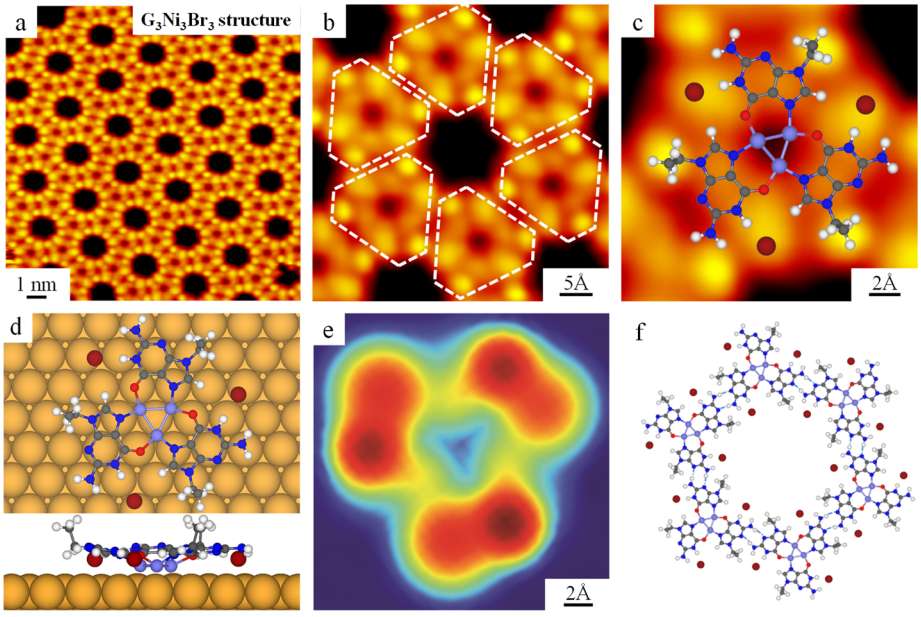

Figure 3. Formation of the $G_3Ni_3Br_3$ network structure after annealing the sample of the $G_3Ni_3Br_4$ phase at 390 K on Au(111). (a) Large-scale STM image showing the honeycomb network composed of the $G_3Ni_3Br_3$ structure. (b) Close-up STM image showing the details of the structure in which $G_3Ni_3Br_3$ structures are indicated by white contours. (c) Further zoomed-in STM image of the $G_3Ni_3Br_3$ motif superimposed with the DFT-optimized gas-phase model. (d) Top and side views of the DFT-relaxed model of the $G_3Ni_3Br_3$ motif on Au(111). (e) ESQC calculated STM image of the $G_3Ni_3Br_3$ motif at E_f. (f) DFT-optimized gas-phase model of the $G_3Ni_3Br_3$ network structure.

Figure 2a). The resulting spectral map along the line (shown as a vertical axis in Figure 2c, with the colors representing the dI/dV intensity) shows that the zero-bias resonances are localized within the range of the metal centers. Furthermore, these resonances are unaffected by the proximity of edges or defects, suggesting that the coupling between neighboring metal–organic motifs is negligibly small.[41]

After a thermal treatment of the sample at 390 K for 10 min, a honeycomb network like the one shown in Figure 3a is observed instead. Close-up STM images resolve that these structures are formed by the elementary triangular motifs, depicted by white contours in Figure 3b. These motifs are assigned to $G_3Ni_3Br_3$ clusters, according to the identical configuration of the $G_3Ni_3I_3$ honeycomb network structure in our previous study.[47] Also note that this structure coincides with the $G_3Ni_3Br_4$ motif from above, but with the on-top Br atoms removed probably due to the annealing process. A further zoomed-in STM image superimposed with the DFT-optimized gas-phase model is shown in Figure 3c. It is noticeable that the electronic density of states of the Ni_3 cluster within the $G_3Ni_3Br_3$ motif is less pronounced in comparison with that in the case of $G_3Ni_3I_3$. The top and side views of the DFT-optimized structural model of $G_3Ni_3Br_3$ on Au(111) are shown in Figure 3d. We find that here the Ni_3 cluster lies 0.3 Å closer to the Au(111) surface than in the $G_3Ni_3Br_4$ motif, presumably suffering a larger hybridization with metal states. The corresponding ESQC calculated STM image is shown in Figure 3e, assigning the peripheral bright spots to ethyl groups pointing upward and to the close-by Br adatoms. The elementary $G_3Ni_3Br_3$ motifs further interact with each other by double hydrogen bonds, resulting in the formation of the honeycomb network shown in Figure 3f.

In contrast to $G_3Ni_3Br_4$, dI/dV spectra obtained at the center of the $G_3Ni_3Br_3$ motif (*i.e.*, the spectrum in Figure 4b taken over the black cross in Figure 4a) show a relatively

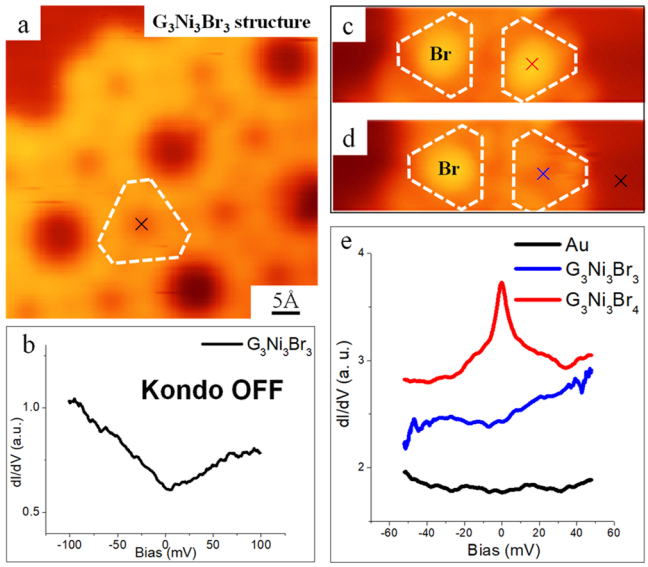

Figure 4. Characterization of the electronic properties of the $G_3Ni_3Br_3$ structure. (a) STM image with a $G_3Ni_3Br_3$ motif highlighted by the white contour. (b) Representative experimental dI/dV point spectrum obtained at the black cross shown in (a), which shows the pronounced Kondo peak vanishes. (c,d) *In situ* STM manipulation to remove the on-top Br atom in the $G_3Ni_3Br_4$ motif (by a bias ramping to ~3.2 V). (e) dI/dV spectra acquired at three points, with the Br atom on top (red), without the Br atom (blue), and on the bare surface (black) (open-feedback parameters: V_t = 1.0 V, I_t = 1 nA, modulation voltage V_{rms} = 0.4 mV, lock-in frequency = 760 Hz).

featureless curve near the zero bias (Figure 4b), which indicates the absence of a Kondo effect upon removal of the on-top Br atom. These results suggest that the magnetic moment concluded after the Kondo resonance in $G_3Ni_3Br_4$

DOI: 10.1021/acsnano.9b04715
ACS Nano 2019, 13, 9936–9943

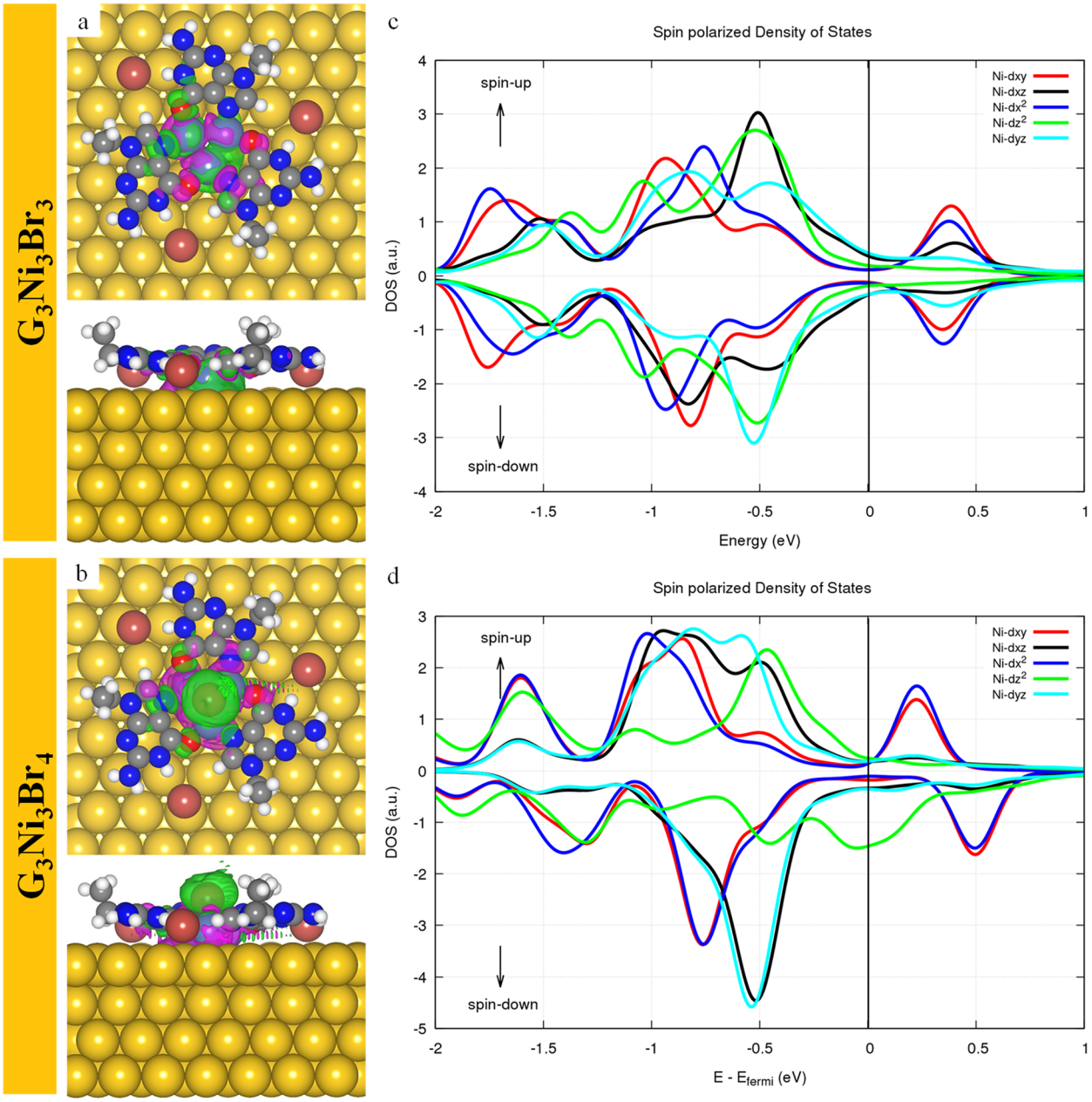

Figure 5. Top and side views of the spin-density of (a) $G_3Ni_3Br_3$ and (b) $G_3Ni_3Br_4$ motifs on the Au(111) surface. The spin-up and spin-down states are drawn as purple and green contours, respectively. The value of isosurfaces are $\pm 1 \times 10^{-4}$ e/Å^3. The SPDOS of the 3d states of the Ni_3 cluster within the (c) $G_3Ni_3Br_3$ and (d) $G_3Ni_3Br_4$ motifs.

clusters is induced by the presence of the Br atom on top of the Ni_3 moiety and vanishes when this halogen atom is removed. By delicately controlling the annealing procedure (at ~380 K for 10 min), an intermediate state composed of both $G_3Ni_3Br_4$ and $G_3Ni_3Br_3$ motifs can be obtained (shown in Figure S2). In this mixed state, dI/dV spectra (Figure S3) further corroborated the coexistence of both magnetic ground states (Kondo ON or OFF) depending on the presence of the Br atom on top. This suggests that the triangular motifs remain at the annealing temperatures, and that the only transformation consists on the detachment of the Br atom from the central part of the motif.

These results suggest that the Kondo state of a molecular $G_3Ni_3Br_4$ cluster could be switched OFF by means of atomic-scale manipulation experiments using the STM. As shown in Figure 4c,d, the STM tip was used to remove the on-top Br atom from a $G_3Ni_3Br_4$ motif, resulting in the formation of the $G_3Ni_3Br_3$ one. Correspondingly, the characteristic Kondo peak (red curve in Figure 4e) of a $G_3Ni_3Br_4$ motif, which is acquired before the manipulation on the species marked in Figure 4c, disappears after removing the on-top Br atom (blue curve acquired at the center of the resulting $G_3Ni_3Br_3$ motif in Figure 4d).

To understand the underlying mechanism behind the formation of a net magnetic moment induced by the on-top Br atom and its disappearance on the $G_3Ni_3Br_3$ motifs, extensive DFT calculations were performed. The incorporation of a Br atom on top of a $G_3Ni_3Br_3$ cluster is accompanied by a net energy gain of 1.4 eV. The Br atom binds to the three Ni atoms and slightly pulls them upward away from the surface by

DOI: 10.1021/acsnano.9b04715
ACS Nano 2019, 13, 9936−9943

0.3 Å, thus reducing their coupling with substrate states. This distortion induces a charge redistribution and builds up a net magnetic moment in the cluster. In Figure 5a,b, the spin densities of the $G_3Ni_3Br_3$ and $G_3Ni_3Br_4$ motifs are depicted, respectively. The spin-up and spin-down states (purple and green contours) are uniformly distributed near the Ni_3 cluster and the Au(111) surface in the $G_3Ni_3Br_3$ motif, whereas in $G_3Ni_3Br_4$ clusters, the spin-up state is significantly more pronounced near the top Br atom. Further analysis shows that, on the Au(111) surface, the magnetic moments of the $G_3Ni_3Br_3$ and $G_3Ni_3Br_4$ motifs are −0.05 and 0.88 μB, respectively. The spin-polarized density of states (SPDOS) on the 3d states of the Ni_3 cluster show that the $3d_{z^2}$ states in the $G_3Ni_3Br_4$ clearly shift upward, partially crossing the Fermi level (Figure 5d) in comparison with that in the $G_3Ni_3Br_3$ (Figure 5c). Thus, the attachment of a Br atom on top induces a charge redistribution described by a partial depopulation of d_{z^2} electrons, which are transferred toward Br states. In fact, the SPDOS on the p orbitals of the on-top Br atom shows a spin-polarized state, as well (Figure S4a, where the bonding configuration between top Br and Ni trimer is also described). Further charge differential analysis also indicates that the on-top Br atom bonds to the Ni_3 cluster with the Br $4p_z$ orbital (Figure S4b). Thus, the enhanced Br $4p_z$ and Ni $3d_{z^2}$ states due to the formation of Br−Ni bonds may be the origin of the apparition of a net magnetic moment, explaining the observation of a Kondo resonance in our experiment.

CONCLUSIONS

In summary, here, we presented an STM manipulation strategy for controlling the spin of the metallic clusters embedded in a metal−organic structure consisting of the attachment of halogen atoms on top. From a combination of high-resolution STM imaging/manipulation and STS measurements, we have demonstrated that the metal−organic motifs containing Ni trimers lie in a magnetic ground state and exhibit a zero-bias Kondo resonance. Compared to a related structure appearing at higher temperatures with no magnetic fingerprint, we deduce that the magnetic state is promoted by the presence of a Br atom on top of the Ni trimer. Controllable removal of the on-top Br atom leads to the disappearance of the magnetic fingerprint from the spectra. Such an experimentally observed Kondo ON state is theoretically attributed to the enhanced Br $4p_z$ and Ni $3d_{z^2}$ states due to the charge redistribution upon the on-top Br adsorption. The finding of the magnetic state for the Ni trimer could be the basis for the bottom-up assembly of high-spin systems, stabilized by a metal−organic framework structure. The spin-manipulation strategy achieved by coordinative interactions of axial halogen atoms presented here provides the possibility to explore the halogen-driven spin switch in more generalized situations, which is of importance in designing spin-tunable interfaces composed of well-defined metal−organic structures with potential applications for spintronic devices.

METHODS

The Au(111) substrate was prepared by several cycles of 1.5 keV Ar^+ sputtering followed by annealing at 820 K for 15 min, resulting in clean and flat terraces separated by monatomic steps. The 9eG molecules (purchased from Sigma-Aldrich, purity >98%) and $NiBr_2$ salt (purchased from Sigma-Aldrich, purity >99%) were loaded into separate cells of the crucible in the molecular evaporator oriented to the substrate. After a thorough degassing, the molecules and salt were deposited onto the Au(111) substrate by thermal sublimation at 440 and 580 K, respectively. The sample was thereafter transferred within the ultrahigh vacuum (UHV) chamber to the STM.

STM images in Figure 1, Figure 3, and Figure S2 were acquired in a UHV chamber (base pressure 1×10^{-10} mbar) equipped with a variable-temperature, fast scanning "Aarhus-type" STM using electrochemically etched W tips purchased from SPECS,[52,53] where measurements were carried out at ∼100−150 K. Scanning conditions were as follows: I_t = 0.5−0.8 nA, V_t = ∼1200 mV. The other STM images and all spectra were acquired on a home-built, low-temperature STM under UHV at pressures of $\sim 1 \times 10^{-11}$ mbar and a base temperature of 4.8 K. Scanning conditions were as follows: I_t = 20 pA, V_t = ∼1000 mV. All of the STM images were further smoothed to eliminate noises. The dI/dV measurements were acquired using a lock-in amplifier technique. Analysis of STS data was performed with Origin and SpectraFox software packages.[54]

The structural optimizations and electronic structures of all systems were obtained with the spin-polarized DFT calculations by using the Vienna *ab initio* simulation package.[55] The electron−ion interactions were described with the projector-augmented wave potentials.[56] The exchange-correlation interactions of electrons were taken account using the Perdew−Burke−Enzerhof of the generalized gradient approximation pseudopotentials.[57] The van der Waals interactions were described with the vdW-D3 method.[58] The cutoff energy of the plane wave basis was set as 400 eV. The gold surfaces were modeled with a periodic slab consisting of four atomic Au layers, in which the bottom two layers were fixed. All other atoms were optimized until the atomic force was less than 0.01 eV per angstrom. A vacuum layer of 20 Å was used to avoid the periodic image interactions. The Brillouin zone of reciprocal space was modeled based on the Γ-centered Monkhorst−Pack scheme, where a 3 × 3 × 1 grid was adopted in geometry optimizations and calculations of electronic properties.[59]

The calculated STM images were obtained by using the ESQC code.[60] Here, the STM junction comprising the substrate, the adsorbates, the tip apex, and the tip support is fully described at the atomic level. A set of semiempirical extended Hückel orbitals is assigned on each atom site. The scattering of tunnel electrons through the junction is calculated that allows the evaluation of the tunneling current with the Landauer formula. This technique has already proven its reliability with small[61,62] and large[63,64] molecular systems.

ASSOCIATED CONTENT

Supporting Information

The Supporting Information is available free of charge on the ACS Publications website at DOI: 10.1021/acsnano.9b04715.

dI/dV spectra for Kondo ON and OFF states with reference curves taken on the bare Au(111) surface; Fano fitting for Kondo resonance; coexistence of the $G_3Ni_3Br_4$ and $G_3Ni_3Br_3$ motifs; corresponding dI/dV spectra on the coexistent motifs; bonding manner between on-top Br and Ni trimer; PDOS of the p_x, p_y, and p_z states of the top Br atom in a $G_3Ni_3Br_4$ motif and differential charge density of the $G_3Ni_3Br_4$ motif (PDF)

AUTHOR INFORMATION

Corresponding Authors

*E-mail: ji.pascual@nanogune.eu.
*E-mail: xuwei@tongji.edu.cn.

ORCID

Haiping Lin: 0000-0002-9948-7060
Jingcheng Li: 0000-0002-6868-3077
Youyong Li: 0000-0002-5248-2756
Jose Ignacio Pascual: 0000-0002-7152-4747
Wei Xu: 0000-0003-0216-794X

DOI: 10.1021/acsnano.9b04715
ACS Nano 2019, 13, 9936−9943

Author Contributions

[¶]L.X. and H.L. contributed equally to this work.

Notes

The authors declare no competing financial interest.

ACKNOWLEDGMENTS

W.X. acknowledges financial support from the National Natural Science Foundation of China (21622307, 21790351) and the Fundamental Research Funds for the Central Universities. H.L. acknowledges support from the National Natural Science Foundation of China (21771134) and the Collaborative Innovation Center of Suzhou Nano Science & Technology, the Priority Academic Program Development of Jiangsu Higher Education Institutions (PAPD), the 111 Project. J.I.P. acknowledges financial support from the Spanish AEI (MAT2016-78293-C6 and the Maria de Maeztu Units of Excellence Program MDM-2016-0618).

REFERENCES

(1) Bogani, L.; Wernsdorfer, W. Molecular Spintronics Using Single-Molecule Magnets. *Nat. Mater.* **2008**, *7*, 179−186.
(2) Moth-Poulsen, K.; Bjørnholm, T. Molecular Electronics with Single Molecules in Solid-State Devices. *Nat. Nanotechnol.* **2009**, *4*, 551−556.
(3) Rocha, A. R.; García-Suárez, V. M.; Bailey, S. W.; Lambert, C. J.; Ferrer, J.; Sanvito, S. Towards Molecular Spintronics. *Nat. Mater.* **2005**, *4*, 335−339.
(4) Candini, A.; Klyatskaya, S.; Ruben, M.; Wernsdorfer, W.; Affronte, M. Graphene Spintronic Devices with Molecular Nanomagnets. *Nano Lett.* **2011**, *11*, 2634−2639.
(5) Liu, L.; Yang, K.; Jiang, Y.; Song, B.; Xiao, W.; Li, L.; Zhou, H.; Wang, Y.; Du, S.; Ouyang, M.; Hofer, W. A.; Castro Neto, A. H.; Gao, H.-J. Reversible Single Spin Control of Individual Magnetic Molecule by Hydrogen Atom Adsorption. *Sci. Rep.* **2013**, *3*, 1210.
(6) Kondo, J. Resistance Minimum in Dilute Magnetic Alloys. *Prog. Theor. Phys.* **1964**, *32*, 37−49.
(7) Kondo, J. Effect of Ordinary Scattering on Exchange Scattering from Magnetic Impurity in Metals. *Phys. Rev.* **1968**, *169*, 437−440.
(8) Li, J.; Schneider, W.-D.; Berndt, R.; Delley, B. Kondo Scattering Observed at a Single Magnetic Impurity. *Phys. Rev. Lett.* **1998**, *80*, 2893−2896.
(9) Madhavan, V.; Chen, W.; Jamneala, T.; Crommie, M. F.; Wingreen, N. S. Tunneling into a Single Magnetic Atom: Spectroscopic Evidence of the Kondo Resonance. *Science* **1998**, *280*, 567−569.
(10) Houck, A. A.; Labaziewicz, J.; Chan, E. K.; Folk, J. A.; Chuang, I. L. Kondo Effect in Electromigrated Gold Break Junctions. *Nano Lett.* **2005**, *5*, 1685−1688.
(11) Frisenda, R.; Gaudenzi, R.; Franco, C.; Mas-Torrent, M.; Rovira, C.; Veciana, J.; Alcon, I.; Bromley, S. T.; Burzurí, E.; van der Zant, H. S. J. Kondo Effect in a Neutral and Stable All Organic Radical Single Molecule Break Junction. *Nano Lett.* **2015**, *15*, 3109−3114.
(12) Kogan, A.; Amasha, S.; Kastner, M. A. Photon-Induced Kondo Satellites in a Single-Electron Transistor. *Science* **2004**, *304*, 1293−1295.
(13) Goldhaber-Gordon, D.; Shtrikman, H.; Mahalu, D.; Abusch-Magder, D.; Meirav, U.; Kastner, M. A. Kondo Effect in a Single-Electron Transistor. *Nature* **1998**, *391*, 156−159.
(14) Parks, J. J.; Champagne, A. R.; Costi, T. A.; Shum, W. W.; Pasupathy, A. N.; Neuscamman, E.; Flores-Torres, S.; Cornaglia, P. S.; Aligia, A. A.; Balseiro, C. A.; Chan, G. K.-L.; Abruña, H. D.; Ralph, D. C. Mechanical Control of Spin States in Spin-1 Molecules and the Underscreened Kondo Effect. *Science* **2010**, *328*, 1370−1373.
(15) Liang, W.; Shores, M. P.; Bockrath, M.; Long, J. R.; Park, H. Kondo Resonance in a Single-Molecule Transistor. *Nature* **2002**, *417*, 725−729.
(16) Park, J.; Pasupathy, A. N.; Goldsmith, J. I.; Chang, C.; Yaish, Y.; Petta, J. R.; Rinkoski, M.; Sethna, J. P.; Abruña, H. D.; McEuen, P. L.; Ralph, D. C. Coulomb Blockade and the Kondo Effect in Single-Atom Transistors. *Nature* **2002**, *417*, 722−725.
(17) Yu, L. H.; Natelson, D. The Kondo Effect in C_{60} Single-Molecule Transistors. *Nano Lett.* **2004**, *4*, 79−83.
(18) Nygård, J.; Cobden, D. H.; Lindelof, P. E. Kondo Physics in Carbon Nanotubes. *Nature* **2000**, *408*, 342−346.
(19) Cervetti, C.; Rettori, A.; Pini, M. G.; Cornia, A.; Repolles, A.; Luis, F.; Dressel, M.; Rauschenbach, S.; Kern, K.; Burghard, M.; Bogani, L. The Classical and Quantum Dynamics of Molecular Spins on Graphene. *Nat. Mater.* **2016**, *15*, 164−168.
(20) Li, J.; Sanz, S.; Corso, M.; Choi, D. J.; Peña, D.; Frederiksen, T.; Pascual, J. I. Single Spin Localization and Manipulation in Graphene Open-Shell Nanostructures. *Nat. Commun.* **2019**, *10*, 200.
(21) Ternes, M.; Heinrich, A. J.; Schneider, W. D. Spectroscopic Manifestations of the Kondo Effect on Single Adatoms. *J. Phys.: Condens. Matter* **2009**, *21*, 053001.
(22) Heinrich, A. J.; Gupta, J. A.; Lutz, C. P.; Eigler, D. M. Single-Atom Spin-Flip Spectroscopy. *Science* **2004**, *306*, 466−469.
(23) Baumann, S.; Paul, W.; Choi, T.; Lutz, C. P.; Ardavan, A.; Heinrich, A. J. Electron Paramagnetic Resonance of Individual Atoms on a Surface. *Science* **2015**, *350*, 417−420.
(24) Knorr, N.; Schneider, M. A.; Diekhöner, L.; Wahl, P.; Kern, K. Kondo Effect of Single Co Adatoms on Cu Surfaces. *Phys. Rev. Lett.* **2002**, *88*, 386−389.
(25) Wahl, P.; Diekhöner, L.; Schneider, M. A.; Vitali, L.; Wittich, G.; Kern, K. Kondo Temperature of Magnetic Impurities at Surfaces. *Phys. Rev. Lett.* **2004**, *93*, 176603.
(26) Schneider, M. A.; Vitali, L.; Wahl, P.; Knorr, N.; Diekhöner, L.; Wittich, G.; Vogelgesang, M.; Kern, K. Kondo State of Co Impurities at Noble Metal Surfaces. *Appl. Phys. A: Mater. Sci. Process.* **2005**, *80*, 937−941.
(27) Schuh, T.; Miyamachi, T.; Gerstl, S.; Geilhufe, M.; Hoffmann, M.; Ostanin, S.; Hergert, W.; Ernst, A.; Wulfhekel, W. Magnetic Excitations of Rare Earth Atoms and Clusters on Metallic Surfaces. *Nano Lett.* **2012**, *12*, 4805−4809.
(28) Otte, A. F.; Ternes, M.; von Bergmann, K.; Loth, S.; Brune, H.; Lutz, C. P.; Hirjibehedin, C. F.; Heinrich, A. J. The Role of Magnetic Anisotropy in the Kondo Effect. *Nat. Phys.* **2008**, *4*, 847−850.
(29) Zhao, A.; Li, Q.; Chen, L.; Xiang, H.; Wang, W.; Pan, S.; Wang, B.; Xiao, X.; Yang, J.; Hou, J. G.; Zhu, Q. Controlling the Kondo Effect of an Adsorbed Magnetic Ion through Its Chemical Bonding. *Science* **2005**, *309*, 1542−1544.
(30) Li, R.; Li, N.; Wang, H.; Weismann, A.; Zhang, Y.; Hou, S.; Wu, K.; Wang, Y. Tuning the Spin-Related Transport Properties of FePc on Au(111) through Single-Molecule Chemistry. *Chem. Commun.* **2018**, *54*, 9135−9138.
(31) Heinrich, B. W.; Ahmadi, G.; Müller, V. L.; Braun, L.; Pascual, J. I.; Franke, K. J. Change of the Magnetic Coupling of a Metal-Organic Complex with the Substrate by a Stepwise Ligand Reaction. *Nano Lett.* **2013**, *13*, 4840−4843.
(32) Li, J.; Merino-Díez, N.; Carbonell-Sanromà, E.; Vilas-Varela, M.; de Oteyza, D. G.; Peña, D.; Corso, M.; Pascual, J. I. Survival of Spin State in Magnetic Porphyrins Contacted by Graphene Nanoribbons. *Sci. Adv.* **2018**, *4*, No. eaaq0582.
(33) Li, J.; Friedrich, N.; Merino, N.; de Oteyza, D. G.; Peña, D.; Jacob, D.; Pascual, J. I. Electrically Addressing the Spin of a Magnetic Porphyrin through Covalently Connected Graphene Electrodes. *Nano Lett.* **2019**, *19*, 3288−3294.
(34) Heinrich, B. W.; Ehlert, C.; Hatter, N.; Braun, L.; Lotze, C.; Saalfrank, P.; Franke, K. J. Control of Oxidation and Spin State in a Single-Molecule Junction. *ACS Nano* **2018**, *12*, 3172−3177.
(35) Iancu, V.; Deshpande, A.; Hla, S.-W. Manipulation of the Kondo Effect *via* Two-Dimensional Molecular Assembly. *Phys. Rev. Lett.* **2006**, *97*, 266603.
(36) Heinrich, B. W.; Braun, L.; Pascual, J. I.; Franke, K. J. Tuning the Magnetic Anisotropy of Single Molecules. *Nano Lett.* **2015**, *15*, 4024−4028.

DOI: 10.1021/acsnano.9b04715
ACS Nano 2019, 13, 9936−9943

(37) Gao, L.; Ji, W.; Hu, Y. B.; Cheng, Z. H.; Deng, Z. T.; Liu, Q.; Jiang, N.; Lin, X.; Guo, W.; Du, S. X.; Hofer, W. A.; Xie, X. C.; Gao, H.-J. Site-Specific Kondo Effect at Ambient Temperatures in Iron-Based Molecules. *Phys. Rev. Lett.* **2007**, *99*, 106402.
(38) Minamitani, E.; Tsukahara, N.; Matsunaka, D.; Kim, Y.; Takagi, N.; Kawai, M. Symmetry-Driven Novel Kondo Effect in a Molecule. *Phys. Rev. Lett.* **2012**, *109*, 086602.
(39) Franke, K. J.; Schulze, G.; Pascual, J. I. Competition of Superconducting Phenomena and Kondo Screening at the Nanoscale. *Science* **2011**, *332*, 940−944.
(40) Girovsky, J.; Nowakowski, J.; Ali, M. E.; Baljozovic, M.; Rossmann, H. R.; Nijs, T.; Aeby, E. A.; Nowakowska, S.; Siewert, D.; Srivastava, G.; Wäckerlin, C.; Dreiser, J.; Decurtins, S.; Liu, S.-X.; Oppeneer, P. M.; Jung, T. A.; Ballav, N. Long-Range Ferrimagnetic Order in a Two-Dimensional Supramolecular Kondo Lattice. *Nat. Commun.* **2017**, *8*, 15388.
(41) Tsukahara, N.; Shiraki, S.; Itou, S.; Ohta, N.; Takagi, N.; Kawai, M. Evolution of Kondo Resonance from a Single Impurity Molecule to the Two-Dimensional Lattice. *Phys. Rev. Lett.* **2011**, *106*, 187201.
(42) Gopakumar, T. G.; Tang, H.; Morillo, J.; Berndt, R. Transfer of Cl Ligands between Adsorbed Iron Tetraphenylporphyrin Molecules. *J. Am. Chem. Soc.* **2012**, *134*, 11844−11847.
(43) Tsukahara, N.; Minamitani, E.; Kim, Y.; Kawai, M.; Takagi, N. Controlling Orbital-Selective Kondo Effects in a Single Molecule through Coordination Chemistry. *J. Chem. Phys.* **2014**, *141*, 054702.
(44) Stróżecka, A.; Soriano, M.; Pascual, J. I.; Palacios, J. J. Reversible Change of the Spin State in a Manganese Phthalocyanine by Coordination of CO Molecule. *Phys. Rev. Lett.* **2012**, *109*, 147202.
(45) Wäckerlin, C.; Tarafder, K.; Girovsky, J.; Nowakowski, J.; Hählen, T.; Shchyrba, A.; Siewert, D.; Kleibert, A.; Nolting, F.; Oppeneer, P. M.; Jung, T. A.; Ballav, N. Ammonia Coordination Introducing a Magnetic Moment in an On-Surface Low-Spin Porphyrin. *Angew. Chem., Int. Ed.* **2013**, *52*, 4568−4571.
(46) Krull, C.; Robles, R.; Mugarza, A.; Gambardella, P. Site- and Orbital-Dependent Charge Donation and Spin Manipulation in Electron-Doped Metal Phthalocyanines. *Nat. Mater.* **2013**, *12*, 337−343.
(47) Xie, L.; Zhang, C.; Ding, Y.; Xu, W. Structural Transformation and Stabilization of Metal-Organic Motifs Induced by Halogen Doping. *Angew. Chem., Int. Ed.* **2017**, *56*, 5077−5081.
(48) Fano, U. Effects of Configuration Interaction on Intensities and Phase Shifts. *Phys. Rev.* **1961**, *124*, 1866−1878.
(49) Nagaoka, K.; Jamneala, T.; Grobis, M.; Crommie, M. F. Temperature Dependence of a Single Kondo Impurity. *Phys. Rev. Lett.* **2002**, *88*, 077205.
(50) Fernández-Torrente, I.; Franke, K. J.; Pascual, J. I. Vibrational Kondo Effect in Pure Organic Charge-Transfer Assemblies. *Phys. Rev. Lett.* **2008**, *101*, 217203.
(51) Moro-Lagares, M.; Korytár, R.; Piantek, M.; Robles, R.; Lorente, N.; Pascual, J. I.; Ibarra, M. R.; Serrate, D. Real Space Manifestations of Coherent Screening in Atomic Scale Kondo Lattices. *Nat. Commun.* **2019**, *10*, 2211.
(52) Besenbacher, F. Scanning Tunnelling Microscopy Studies of Metal Surfaces. *Rep. Prog. Phys.* **1996**, *59*, 1737−1802.
(53) Lægsgaard, E.; Österlund, L.; Thostrup, P.; Rasmussen, P. B.; Stensgaard, I.; Besenbacher, F. A High-Pressure Scanning Tunneling Microscope. *Rev. Sci. Instrum.* **2001**, *72*, 3537−3542.
(54) Ruby, M. SpectraFox: A Free Open-Source Data Management and Analysis Tool for Scanning Probe Microscopy and Spectroscopy. *SoftwareX* **2016**, *5*, 31−36.
(55) Kresse, G.; Furthmuller, J. Efficient Iterative Schemes for *Ab Initio* Total-Energy Calculations Using a Plane-Wave Basis Set. *Phys. Rev. B: Condens. Matter Mater. Phys.* **1996**, *54*, 11169−11186.
(56) Blöchl, P. E. Projector Augmented-Wave Method. *Phys. Rev. B: Condens. Matter Mater. Phys.* **1994**, *50*, 17953−17979.
(57) Perdew, J. P.; Burke, K.; Ernzerhof, M. Generalized Gradient Approximation Made Simple. *Phys. Rev. Lett.* **1996**, *77*, 3865−3868.
(58) Grimme, S.; Antony, J.; Ehrlich, S.; Krieg, H. A Consistent and Accurate *Ab Initio* Parametrization of Density Functional Dispersion Correction (DFT-D) for the 94 Elements H-Pu. *J. Chem. Phys.* **2010**, *132*, 154104.
(59) Monkhorst, H. J.; Pack, J. D. Special Points for Brillouin-Zone Integrations. *Phys. Rev. B* **1976**, *13*, 5188−5192.
(60) Sautet, P.; Joachim, C. Calculation of the Benzene on Rhodium STM Images. *Chem. Phys. Lett.* **1991**, *185*, 23−30.
(61) Villagómez, C. J.; Castanié, F.; Momblona, C.; Gauthier, S.; Zambelli, T.; Bouju, X. Adsorption of Single 1,8-Octanedithiol Molecules on Cu(100). *Phys. Chem. Chem. Phys.* **2016**, *18*, 27521−27528.
(62) Yu, M.; Kalashnyk, N.; Barattin, R.; Benjalal, Y.; Hliwa, M.; Bouju, X.; Gourdon, A.; Joachim, C.; Lægsgaard, E.; Besenbacher, F.; Linderoth, T. R. Self-Assembly of Hydrogen-Bonded Chains of Molecular Landers. *Chem. Commun.* **2010**, *46*, 5545−5547.
(63) Xu, W.; Dong, M. D.; Gersen, H.; Vázquez-Campos, S.; Bouju, X.; Lægsgaard, E.; Stensgaard, I.; Crego-Calama, M.; Reinhoudt, D. N.; Linderoth, T. R.; Besenbacher, F. Exploring the Transferability of Large Supramolecular Assemblies to the Vacuum-Solid Interface. *Nano Res.* **2009**, *2*, 535−542.
(64) Villagomez, C. J.; Guillermet, O.; Goudeau, S.; Ample, F.; Xu, H.; Coudret, C.; Bouju, X.; Zambelli, T.; Gauthier, S. Self-Assembly of Enantiopure Domains: The Case of Indigo on Cu(111). *J. Chem. Phys.* **2010**, *132*, 074705.

DOI: 10.1021/acsnano.9b04715
ACS Nano 2019, 13, 9936−9943